

Supporting Information

***In-situ* High-Potential-Driven Surface Restructuring of Ternary AgPd-Pt_{dilute} Aerogels with Record High Performance Improvement for Formate Oxidation Electrocatalysis†**

Jiali Wang,^{a,b} Fuyi Chen,^{*a,b} Yachao Jin,^{a,b} Longfei Guo,^{a,b} Xiaofang Gong,^{a,b} Xiaolu Wang,^{a,b}
and Roy L. Johnston^c

^aState Key Laboratory of Solidification Processing, Northwestern Polytechnical University, Xi'an, 710072, China.

^bSchool of Materials Science and Engineering, Northwestern Polytechnical University, Xi'an, 710072, China.

^cSchool of Chemistry, University of Birmingham, B15 2TT, UK.

*Corresponding author. Tel./fax: +8629-88492052. E-mail address: fuyichen@nwpu.edu.cn

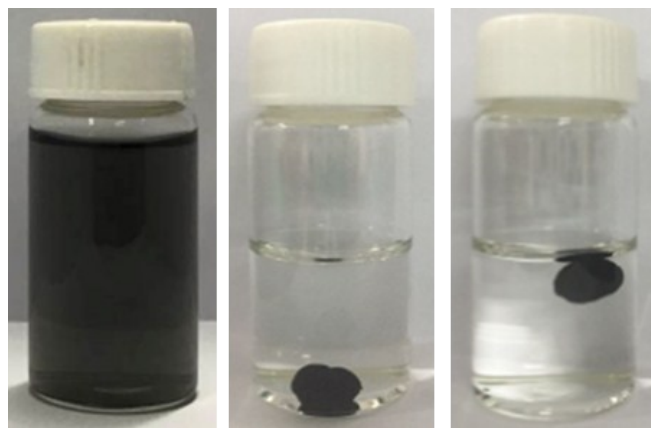


Fig. S1 Digital images of trimetallic AgPd-Pt_{dilute} initial colloid solution (left), corresponding hydrogel formed in water (middle) and washed in NaCl saturated solution (right).

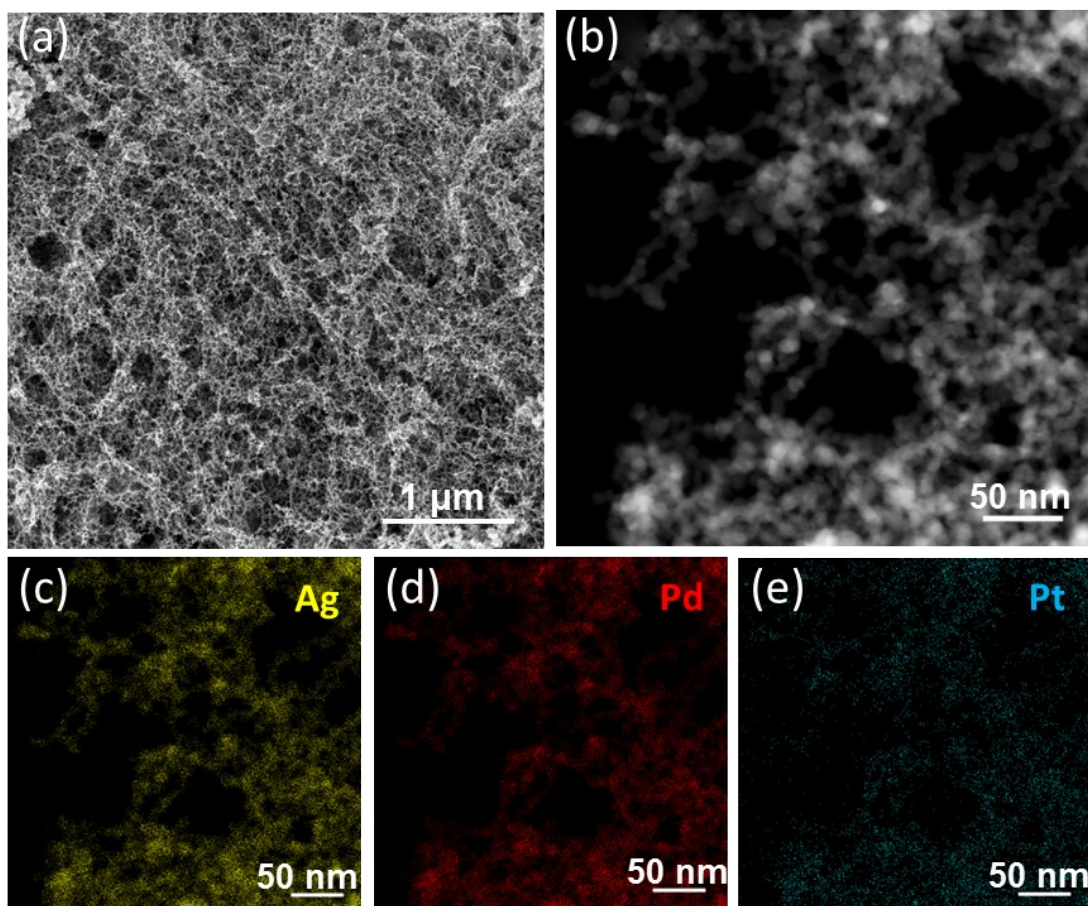


Fig. S2 Physical characterizations of the as-synthesized AgPd-Pt_{dilute} aerogel. (a) SEM image. (b) HAADF-STEM image and (c-e) high-resolution EDS elemental mappings of a randomly-selected area, indicating the uniform distribution of Ag, Pd and Pt in the AgPd-Pt_{dilute} aerogels.

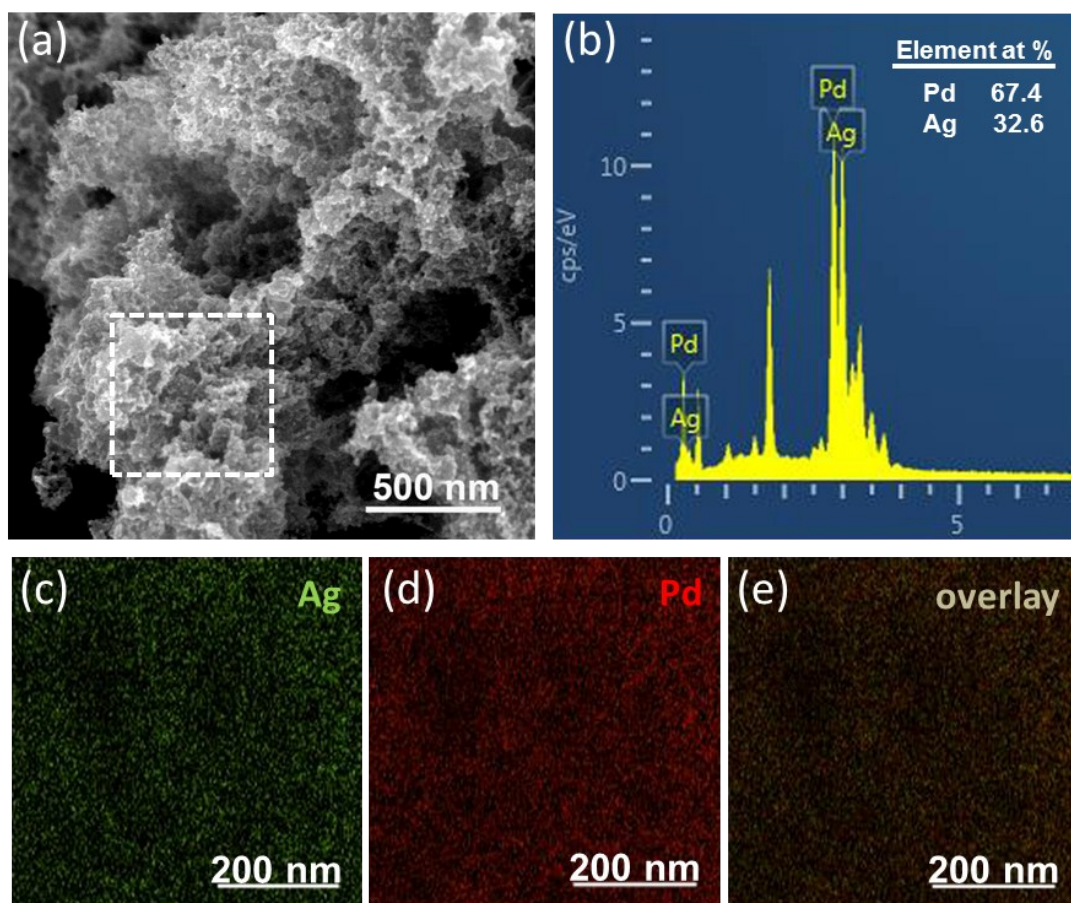


Fig. S3 (a) SEM image of the bimetallic AgPd aerogel with nominal Ag/Pd atomic ratio of 1/2, showing the compactly fused irregular nanoparticles. (b) SEM-EDS spectrum, the atomic ratio of Ag/Pd in the bimetallic AgPd aerogel is in good agreement with the stoichiometry of initial metal precursors, confirming that our strategy is a general and stoichiometry-controllable method. (c-e) The elemental mappings of a randomly-selected area marked in a), showing the evenly distributed Ag and Pd in the AgPd aerogels.

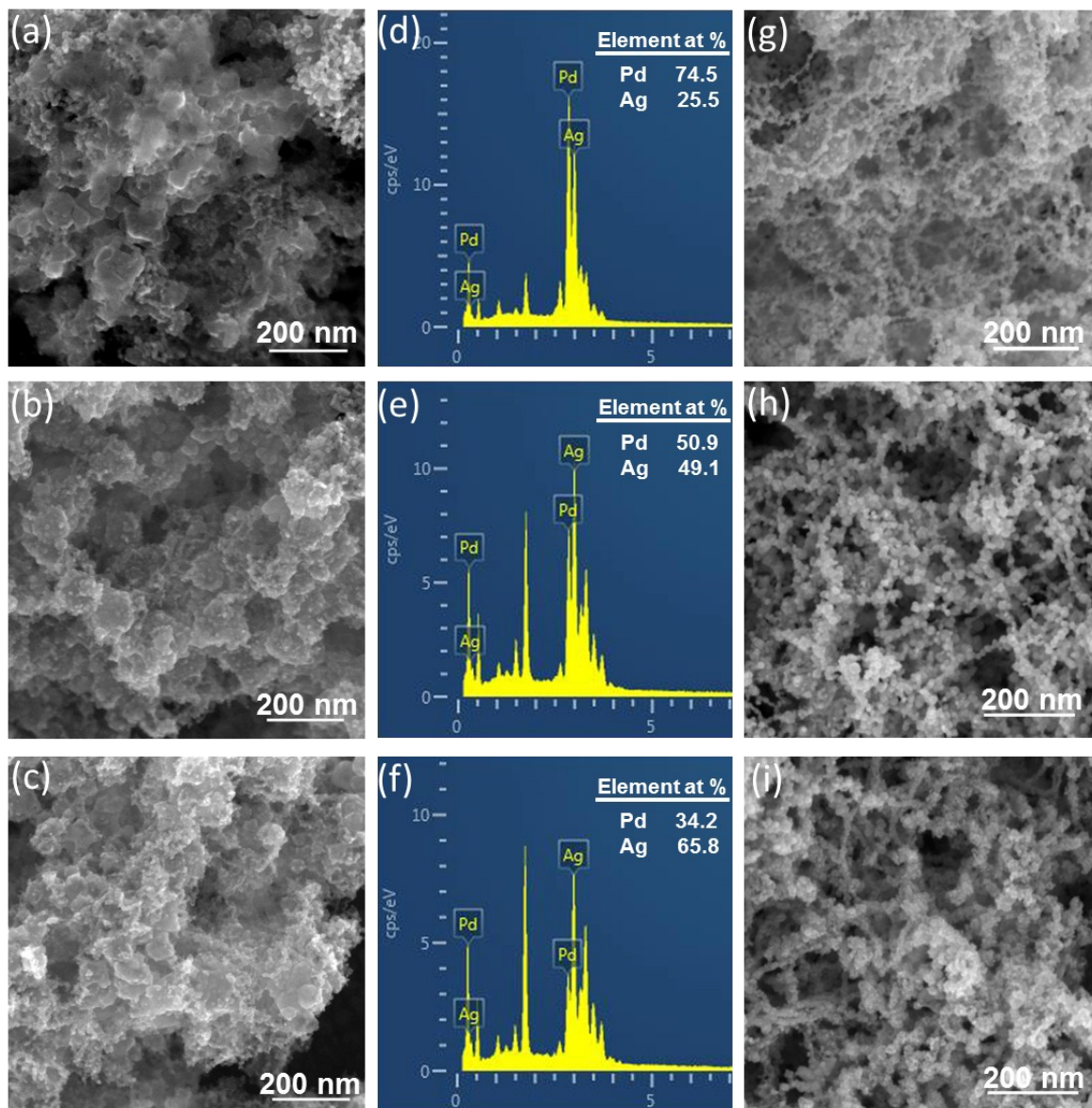


Fig. S4 (a-c) SEM images of bimetallic AgPd aerogels with different Ag/Pd atomic ratio, (a) 1:3, (b) 1:1 and (c) 2:1. (d-f) The corresponding SEM-EDS spectra of bimetallic Ag_xPd_y aerogels, the atomic ratio of Ag/Pd in all the AgPd aerogels is consistent well with the stoichiometry of initial metal precursors. (g-i) The corresponding SEM images of trimetallic Ag_xPd_y-Pt_{dilute} aerogels with the same amount of Pt, showing the obvious morphology transformation from large fused nanoparticles to the interconnected nanowires.

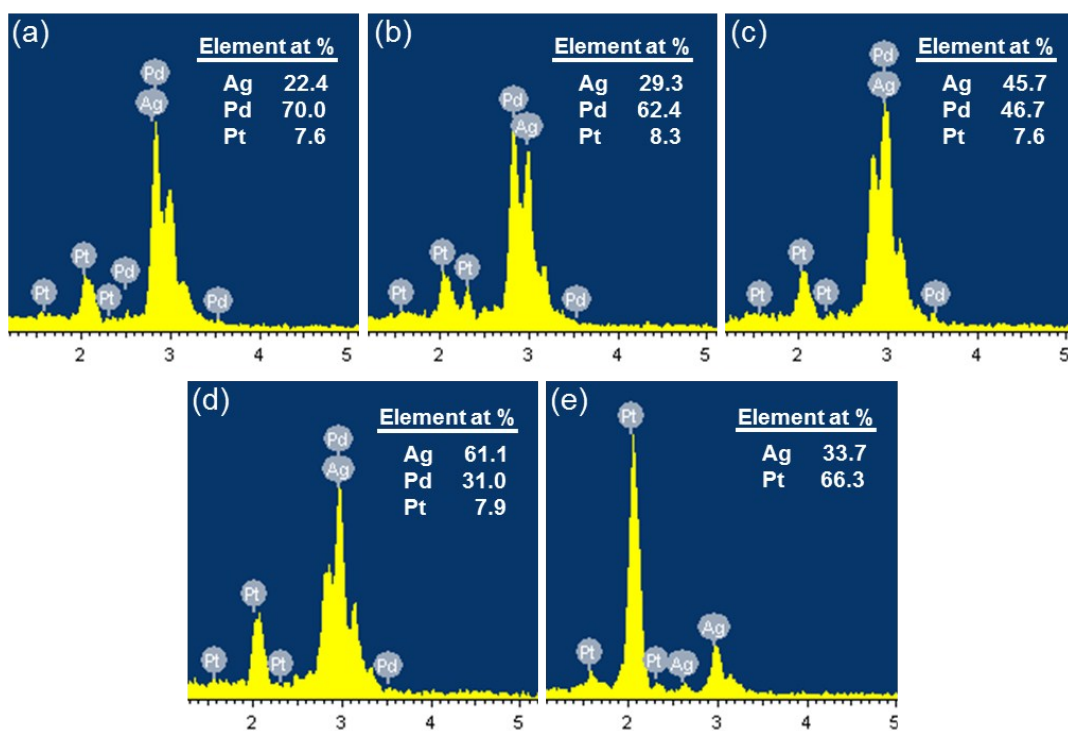


Fig. S5 EDS spectra of trimetallic $\text{Ag}_x\text{Pd}_y\text{-Pt}_{\text{dilute}}$ aerogels with different Ag/Pd atomic ratio of (a) 1:3, (b) 1:2, (c) 1:1, (d) 2:1, and (e) bimetallic Ag_1Pt_2 catalyst.

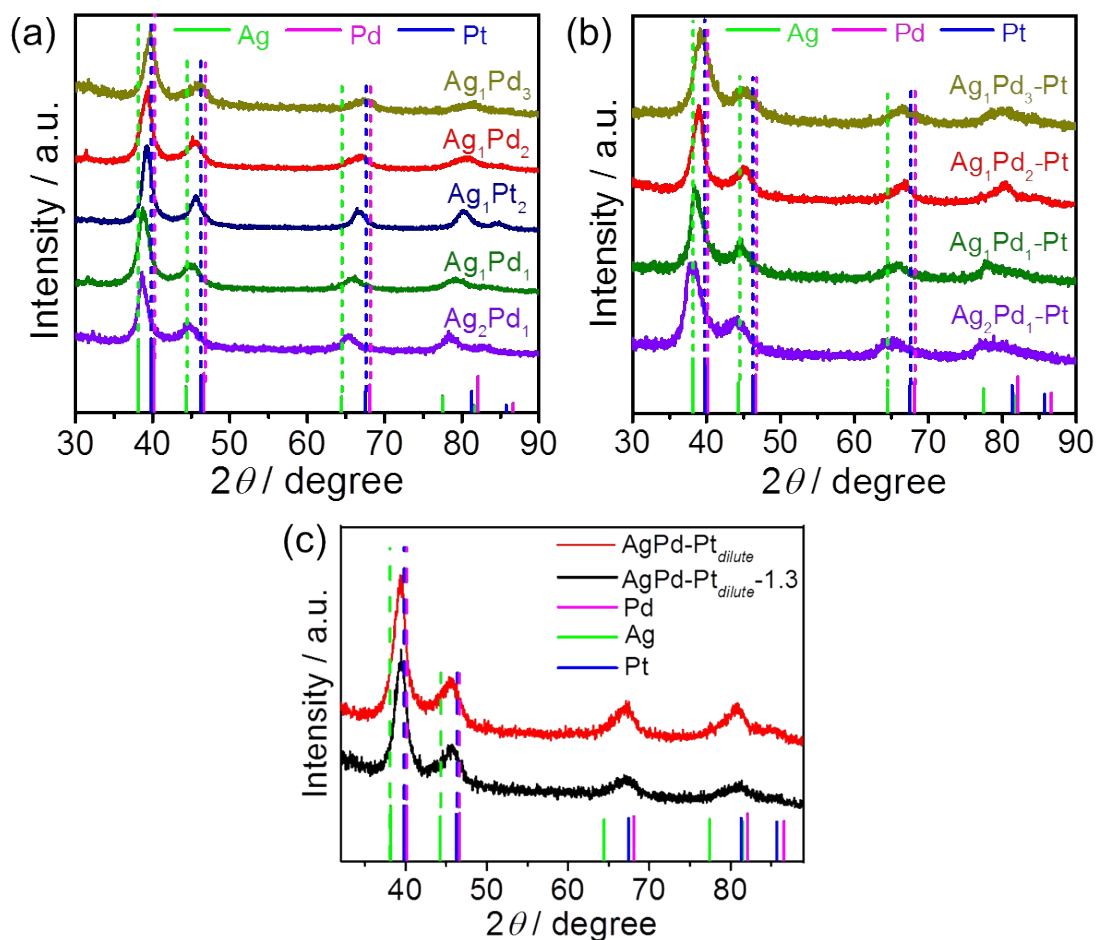


Fig. S6 XRD patterns of (a) bimetallic Ag_xPd_y and Ag_1Pt_2 aerogels and (b) trimetallic Ag_xPd_y-Pt aerogels ($x:y = 1:3, 1:2, 1:1$ and $2:1$). (c) XRD patterns of pristine $AgPd-Pt_{dilute}$ and surface-restructured $AgPd-Pt_{dilute}-1.3$ aerogels. Bar diagram: Ag #04-0783, Pd #46-1043 and Pt #04-0802.

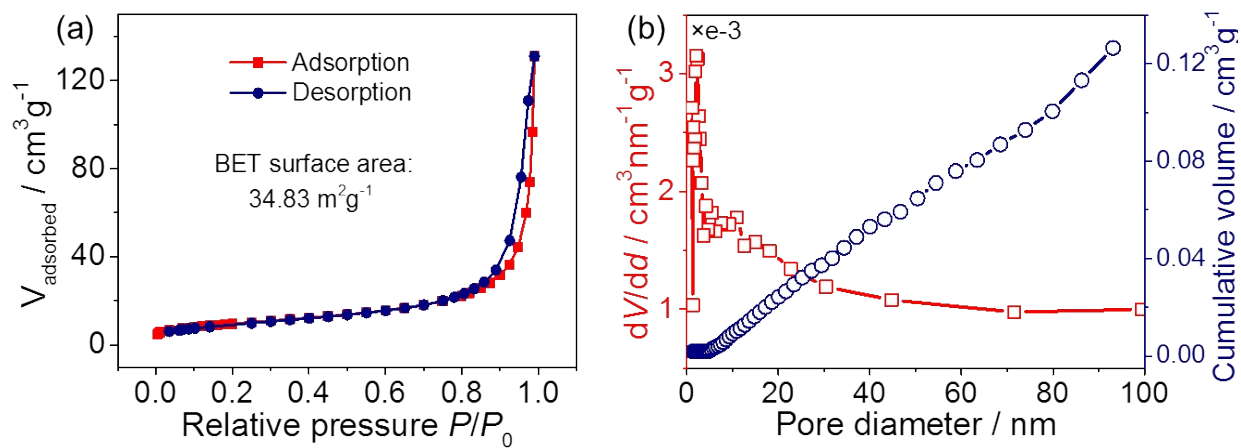


Fig. S7 (a) Nitrogen adsorption/desorption isotherms, (b) pore size distribution and cumulative volume of the as-prepared AgPd-Pt_{dilute} aerogel catalyst.

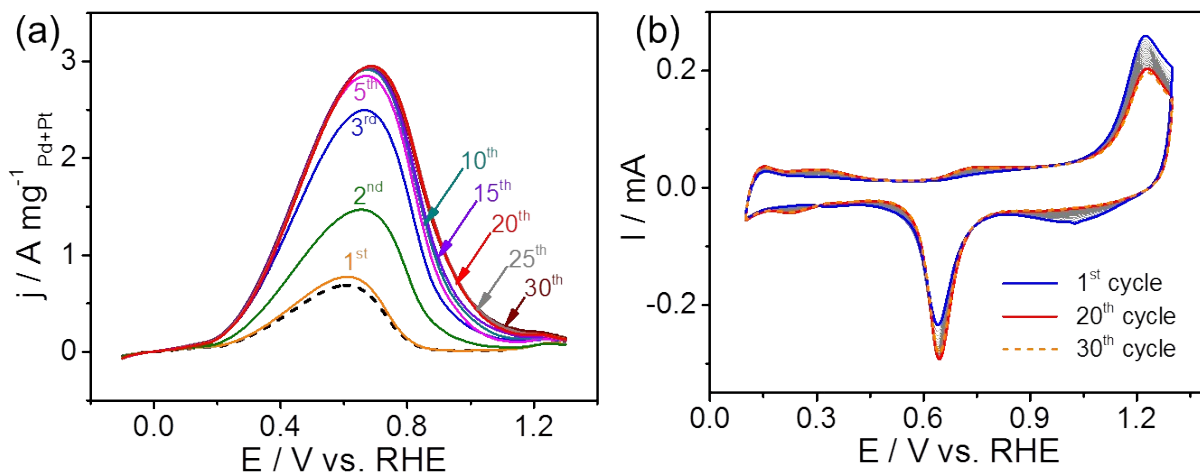


Fig. S8 (a) Forward scan CV curves of AgPd-Pt_{dilute} electrocatalyst in 0.5 M KOH + 0.5 M HCOOK from 1st to 30th potential cycles. (b) CV evolution of AgPd-Pt_{dilute} recorded in pure 0.5 M KOH solution from 1st to 30th potential cycles.

Selecting 20 potential cycles as the optimal cycling number for the activation process are based on the systematically electrochemical results. Firstly, we carried out the CV measurement on AgPd-Pt_{dilute} for formate oxidation for 30 cycles with the large upper potential limit of 1.3 V in 0.5 M KOH + 0.5 M HCOOK solution and plotted the sequential CV curves as shown in Fig. S8a (only forward scan curves of CV were showed for the sake of clarity). The mass current density for FOR on AgPd-Pt_{dilute} shows the remarkable increase with increasing number of the initial 10 potential cycles and shows a slight increase in the following 10 cycles. After the number of the potential cycles increased to 20 cycles, no discernable current enhancement was observed, which indicates that a stable electrocatalytic activity was achieved in the AgPd-Pt_{dilute} catalysts after the activation process of 20 potential cycles. Secondly, we further investigated the electrochemical behaviors of AgPd-Pt_{dilute} during the continuous cycling in pure 0.5 M KOH solution. CV curves in Fig. S8b exhibit that a gradual evolution of the catalyst surface happens with the cycle number continuously

increasing to 20 cycles, while the following CV curves undergo no visible change even though the potential cycling was conducted up to 30 cycles, strongly implying that the AgPd- Pt_{dilute} catalysts experience the significant surface restructuring in the initial 20 cycles, and obtain a stable structure on surface after 20 cycles, which agrees well with the FOR activity results shown in Fig. S8a. On the basis of the aforementioned results, it can be concluded that 20 is the optimal cycle number for activation process to achieve the most stable surface structure and greatly enhanced FOR activity.

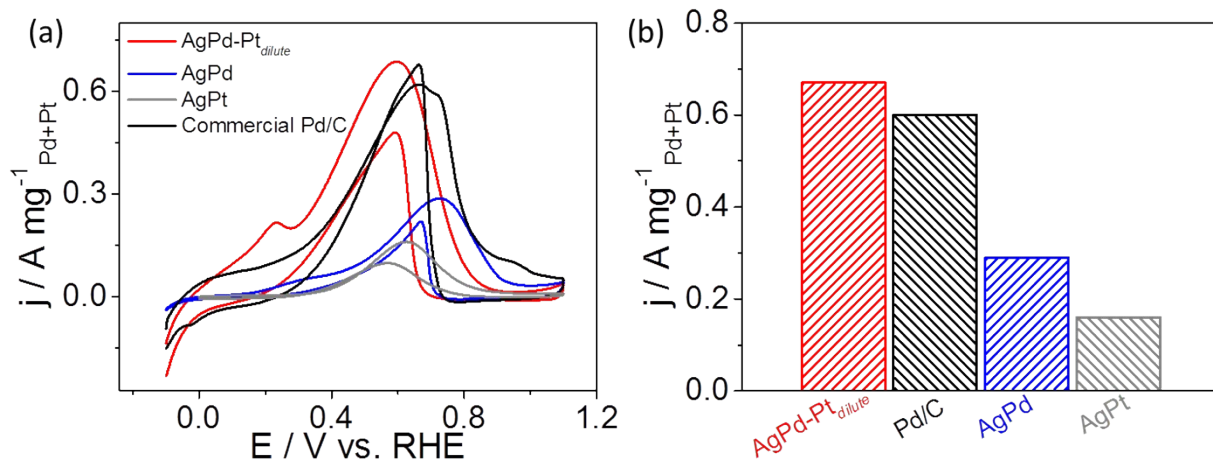


Fig. S9 (a) CV curves of AgPd-Pt_{dilute}, AgPd, AgPt and commercial Pd/C electrocatalysts for FOR in 0.5 M KOH + 0.5 M HCOOK solution with a conventional small potential window (-0.1~1.1 V) at 50 mV s^{-1} . (b) Comparison of the mass peak current density of AgPd-Pt_{dilute}, AgPd, AgPt and commercial Pd/C electrocatalysts.

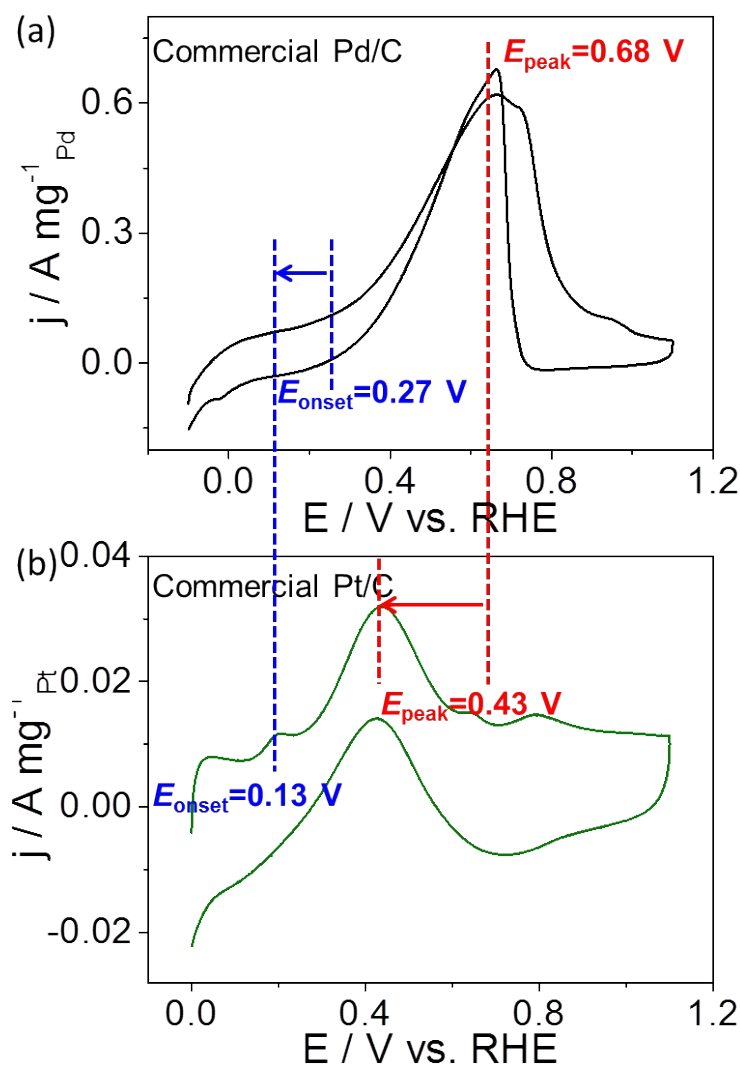


Fig. S10 CV curves of (a) commercial Pd/C and (b) Pt/C electrocatalysts for FOR in 0.5 M KOH + 0.5 M HCOOK solution at 50 mV s⁻¹. The vertical red and blue lines indicate the specific positions of peak and onset potentials, respectively. The commercial Pt/C catalyst exhibits much lower peak current density for FOR compared with the commercial Pd/C (0.61 A mg_{Pd}⁻¹ vs. 0.03 A mg_{Pt}⁻¹), indicating very limited activity of Pt for the formate oxidation in alkaline media. However, the Pt/C catalyst shows much more negative onset and peak potential than that of the Pd/C, it is expected that the incorporation of Pt would play a crucial role in lowering the oxidation potential for Pd-based catalyst.

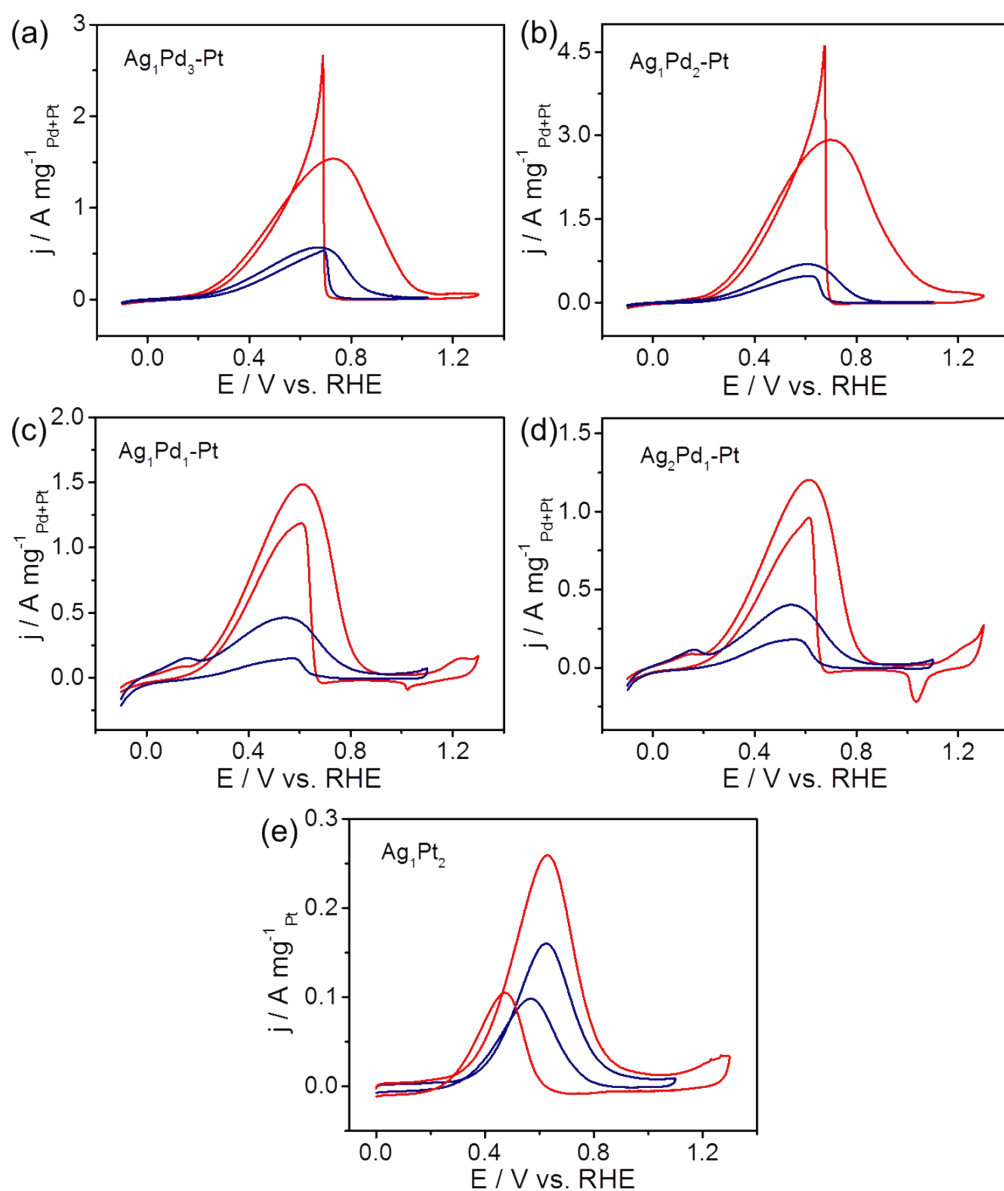


Fig. S11 CV curves of various $\text{Ag}_x\text{Pd}_y\text{-Pt}$ ($x:y = 1:3, 1:2, 1:1$ and $2:1$) and Ag_1Pt_2 electrocatalysts for FOR in $0.5 \text{ M KOH} + 0.5 \text{ M HCOOK}$ solution at a conventional small ($-0.1 \sim 1.1 \text{ V}$, blue line) and large ($-0.1 \sim 1.3 \text{ V}$, red line) potential window.

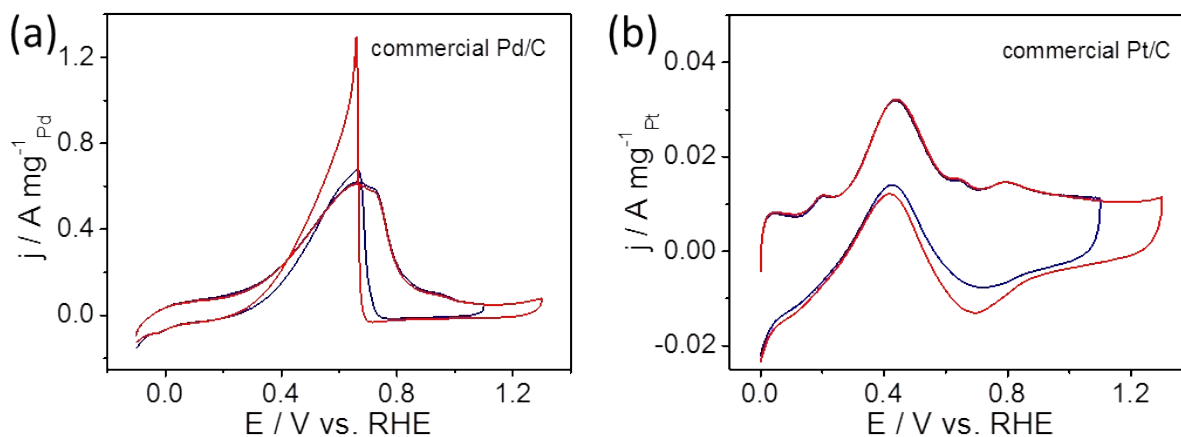


Fig. S12 CV curves of (a) commercial Pd/C and (b) commercial Pt/C electrocatalysts for FOR in 0.5 M KOH + 0.5 M HCOOK solution at a conventional small (-0.1~1.1 V, blue line) and large (-0.1~1.3 V, red line) potential window. It can be seen from the forward potential scans that both monometallic Pd/C and Pt/C catalysts shows no visible activity improvement for FOR when the upper potential limit is enlarged from 1.1 V to 1.3 V during the electrochemical testing, indicating that the redox process of Pd and Pt plays the negligible role for greatly enhanced FOR performance. It should be noted that the backward potential scan recorded with the large upper potential limit of 1.3 V for FOR on Pd/C is strikingly high compared with that recorded with the small upper potential limit of 1.1 V, which is ascribed to the fact that more PdO species on surface are remarkably reduced during the high-potential cycling, exposing more active sites for FOR.

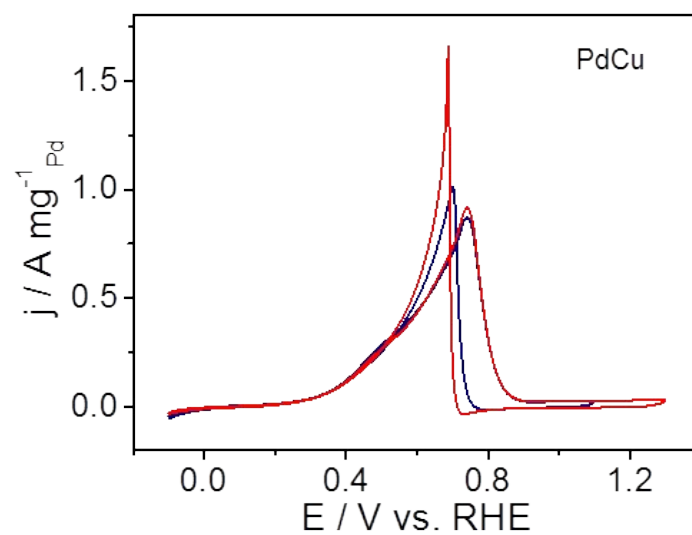


Fig. S13 CV curves of as-synthesized PdCu aerogel electrocatalyst for FOR in 0.5 M KOH + 0.5 M HCOOK solution at a conventional small (-0.1~1.1 V, blue line) and large (-0.1~1.3 V, red line) potential window.

Table S1. The nominal molar ratios of different bimetallic Ag_xPd_y , trimetallic $\text{Ag}_x\text{Pd}_y\text{-Pt}_{\text{dilute}}$ and Ag_1Pt_2 aerogels and the corresponding feed amount in the precursor solution.

Catalyst	H_2PdCl_4 (10 mM)	AgNO_3 (10 mM)	H_2PtCl_6 (10 mM)
Ag_1Pd_3	9 mL	3 mL	-
Ag_1Pd_2 (referred to as AgPd)	8 mL	4 mL	-
Ag_1Pd_1	6 mL	6 mL	-
Ag_2Pd_1	4 mL	8 mL	-
Ag_1Pt_2	-	4 mL	8 mL
$\text{Ag}_1\text{Pd}_3\text{-Pt}$	8.30 mL	2.78 mL	0.92 mL
$\text{Ag}_1\text{Pd}_2\text{-Pt}$ (referred to as AgPd- $\text{Pt}_{\text{dilute}}$)	7.40 mL	3.68 mL	0.92 mL
$\text{Ag}_1\text{Pd}_1\text{-Pt}$	5.52 mL	5.56 mL	0.92 mL
$\text{Ag}_2\text{Pd}_1\text{-Pt}$	3.68 mL	7.40 mL	0.92 mL

Table S2. The elemental compositions obtained by EDS and ICP-OES analysis for different Ag_xPd_y , $\text{Ag}_x\text{Pd}_y\text{-Pt}_{dilute}$ and Ag_1Pt_2 aerogels.

Nominal Composition / at %	EDS analysis / at %			ICP-OES analysis / at %		
	Ag	Pd	Pt	Ag	Pd	Pt
Ag_1Pd_3	25.5	74.5	-	26.3	73.7	-
Ag_1Pd_2	32.6	67.4	-	33.0	67.0	-
Ag_1Pd_1	49.1	50.9	-	50.4	49.6	-
Ag_2Pd_1	65.8	34.2	-	66.1	33.9	-
Ag_1Pt_2	33.7	-	66.3	32.4	-	67.6
$\text{Ag}_1\text{Pd}_3\text{-Pt}$	22.4	70.0	7.6	23.2	69.1	7.7
$\text{Ag}_1\text{Pd}_2\text{-Pt}$	29.3	62.4	8.3	30.5	61.6	7.9
$\text{Ag}_1\text{Pd}_1\text{-Pt}$	45.7	46.7	7.6	46.0	46.4	7.6
$\text{Ag}_2\text{Pd}_1\text{-Pt}$	61.1	31.0	7.9	59.6	32.3	8.1

Table S3. Comparison of mass peak current density of different catalysts for FOR recorded with a small (1.1 V) and a large (1.3 V) upper potential limit during the electrochemical testing.

Catalyst	$J_{\text{small}} / -0.1 \sim 1.1 \text{ V}$ ($\text{A mg}_{\text{Pd/Pt}}^{-1}$)	$J_{\text{large}} / -0.1 \sim 1.3 \text{ V}$ ($\text{A mg}_{\text{Pd/Pt}}^{-1}$)	$J_{\text{large}} / J_{\text{small}}$
Ag_1Pd_3	0.17	0.50	2.9
Ag_1Pd_2	0.28	1.36	4.9
Ag_1Pd_1	0.11	0.42	3.8
Ag_2Pd_1	0.07	0.23	3.2
Ag_1Pt_2	0.16	0.25	1.5
$\text{Ag}_1\text{Pd}_3\text{-Pt}$	0.57	1.54	2.7
$\text{Ag}_1\text{Pd}_2\text{-Pt}$	0.67	2.94	4.4
$\text{Ag}_1\text{Pd}_1\text{-Pt}$	0.46	1.47	3.2
$\text{Ag}_2\text{Pd}_1\text{-Pt}$	0.40	1.21	3.0
Commercial Pd/C	0.61	0.61	1.0
Commercial Pt/C	0.03	0.03	1.0

Table S4. Summary of catalytic properties of FOR electrocatalysts in the scientific literature.

catalyst name	onset potential	peak potential	SA (mA cm ⁻²)	MA (A mg ⁻¹)	scan rate (mV s ⁻¹)	electrolyte	Ref.
AgPd-Pt _{dioxide} -1.3	0.2 V vs. RHE	0.72 V vs. RHE	3.52	2.94	50	0.5 M KOH+ 0.5 M HCOOK	this work
AgPd-1.3	0.5 V vs. RHE	0.78 V vs. RHE	2.80	1.33	50	0.5 M KOH+ 0.5 M HCOOK	this work
PdAu/Ni foam	-	-0.44 V vs. MMO	0.75	-	50	0.5 M NaOH+ 0.1 M HCOONa	1
Pd/Ni foam	-	-0.41 V vs. MMO	0.39	-	50	0.5 M NaOH+ 0.1 M HCOONa	1
PdCu/C	-0.556 V vs. SHE	-	3.46	-	30	1 M KOH+ 1 M HCOOK	2
A-I-Pd/C	-	-	0.133	-	20	1 M KOH+ 0.1 M HCOOK	3
A-Pd/C	-	-	0.136	-	20	1 M KOH+ 0.1 M HCOOK	3
CuPdAu/C	-	-	-	0.74	50	0.5 M KOH+ 0.5 M HCOOK	4
SCR-CuPdAu/C	-0.6 V vs. SHE	0.05 V vs. SHE	-	1.15	50	0.5 M KOH+ 0.5 M HCOOK	4
PtAg	-	0.66 V vs. RHE	-	0.83	50	1 M KOH+ 1 M HCOOK	5
Pd ₂₃ Co/C	-0.62 V vs. MMO	-	-	2.7	50	1 M KOH+ 1 M HCOOK	6

Abbreviations: MMO: Hg/HgO electrode (1 M KOH, 0.098 V vs. SHE); A-I-Pd/C: ammonia and iodine ion doped Pd/C catalyst; SCR-CuPdAu/C: surface copper removed CuPdAu/C catalyst.

References

- 1 Y. Li, Y. He and W. Yang, *J. Power Sources*, 2015, **278**, 569-573.
- 2 J. Noborikawa, J. Lau, J. Ta, S. Hu, L. Scudiero, S. Derakhshan, S. Ha and J. L. Haan, *Electrochim. Acta*, 2014, **137**, 654-660.
- 3 M. Choun, K. Ham, D. Shin, J. K. Lee and J. Lee, *Catal. Today*, 2017, **295**, 26-31.
- 4 H. Mao, T. Huang and A. Yu, *Int. J. Hydrogen Energy*, 2016, **41**, 13190-13196.
- 5 S.-H. Han, H.-M. Liu, J. Bai, X. L. Tian, B. Y. Xia, J.-H. Zeng, J.-X. Jiang and Y. Chen, *ACS Appl. Energy Mater.*, 2018, **1**, 1252-1258.
- 6 S. Sankar, G. M. Anilkumar, T. Tamaki and T. Yamaguchi, *ACS Appl. Energy Mater.*, 2018, **1**, 4140-4149.